Astron. Astrophys. 339, 477–482 (1998)

ASTRONOMY AND ASTROPHYSICS

Dust distribution in radiation pressure outflow

Application to the BD+31°643 disk

A. Lecavelier des Etangs[1,2], **A. Vidal-Madjar**[2], **and R. Ferlet**[2]

[1] NCRA, TATA Institute of Fundamental Research, Post Bag 3, Ganeshkhind, Pune University Campus, Pune 411 007, India
[2] Institut d'Astrophysique de Paris, CNRS, 98bis Boulevard Arago, F-75014 Paris, France

Received 8 June 1998 / Accepted 8 September 1998

Abstract. The radial distribution of dust has been calculated in outflows driven by radiation pressure in which the gas drag is taken into account. It is shown that the dust distribution in the newly discovered candidate disk around BD+31°643 can be explained by this simple model, provided that the ambient gas of the surrounding cluster IC 348 has a density $\rho \sim 10^4$ cm^{-3}. The dust is probably produced within 2300 AU from the central binary star.

Key words: stars: individual: BD+31°643 – circumstellar matter

1. Introduction

Dust around main sequence stars has been discovered more than a decade ago by the IRAS satellite (Aumann et al. 1984), but little work on the dust dynamics has been done. Moreover until recently, β Pictoris was the only star to capture all the attention, because images showed that the dust shell was in fact a disk seen edge-on from the Earth (Smith & Terrile 1984). These images have given unique information on disk morphology and dust distribution (Artymowicz et al. 1989, Kalas & Jewitt 1995). The dust distribution, the intriguing asymmetries or the wrapped geometry have been studied thoroughly (Roques et al. 1994, Artymowicz 1995, Lecavelier des Etangs et al. 1996a, 1996b, Mouillet et al. 1997). But it is still not clear if these results apply only to the well-known β Pictoris disk or if they describe a general scheme for which β Pictoris is an example.

Recently, the situation changed drastically when Kalas & Jewitt (1997) discovered a candidate dust disk around BD+31°-643. Although it still needs observational follow-up, this detection has been first confirmed by the consistency with polarimetric measurements (Andersson & Wannier 1997). As in the β Pictoris case, the dust lifetime around BD+31°643 is smaller than the age of the star. There must therefore be a replenishment mechanism. The origin of dust (collision or evaporation of parent bodies?) must be identified. It is interesting to see if the analysis of the dynamics and the distribution of the dust can provide new insight on various aspects of the origin and history of dusty disks around main-sequence stars.

If this dust was in fact coming from the interstellar medium and dragged by invisible massive gas, the dynamics of this disk could be very different from the dynamics of the dust around β Pictoris. But, if this disk was really the second member of the β Pictoris family for which we have an image, then this would shed more light on the origin of the β Pictoris-like disks (Lissauer 1997).

In addition, BD+31°643 is a binary star; this could have consequences on possible dust production mechanisms. At least, if this disk is replenished like the β Pictoris one, this shows that the formation of planetesimals is possible around binary stars (Kalas & Jewitt, 1997). The evolution and stability of planetary systems in this environment is starting to be investigated (Brunini 1997, Benest 1998). But knowledge on these putative parent bodies from the observation of dust have to be improved, and a better understanding of the dust dynamics is needed.

In this paper, after a summary of the characteristics of the BD+31°643 candidate disk, where it is recalled that the dust is expelled by the radiation pressure (Sect. 2), we present theoretical calculation on outflows driven by radiation pressure in which the gas drag is taken into account (Sects. 3 and 4). Application to BD+31°643 (Sect. 5) and numerical simulations (Sect. 6) show that the observed dust distribution (or more precisely the surface brightness distribution along the midplane of the disk) can be explained by the ambient gas drag of the cluster IC 348, if the gas density is between 10^3 and 10^5 cm^{-3}.

2. The BD+31°643 disk

The apparent dust surrounding BD+31°643 presents strong similarities with the β Pictoris circumstellar matter, namely a disk-like structure seen edge-on with a scattered light distribution close to a power law. The similarities are clearly visible through a comparison of the morphology of both disks seen on the corresponding images (see Fig. 1 in Kalas & Jewitt, 1997).

But important differences are also found. The observed dust is at significantly larger distances in the case of BD+31°643, simply because the central star is much farther ($\sim$ 330 pc). In the surrounding of BD+31°643, the disk is seen between

Send offprint requests to: A. Lecavelier des Etangs

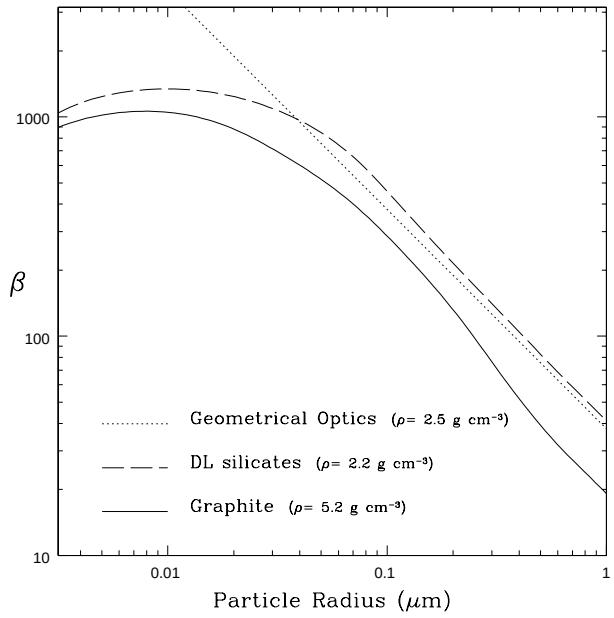

Fig. 1. The ratio of the radiation force to the gravitational force as a function of particle size for "Draine & Lee" silicates (dashed line), graphite (solid line) and the geometrical optics (dotted line)

1300 AU and 6000 AU with a flatter brightness distribution: $F(r) \propto r^{-0.3}$ between 4 and 7 arcsec (1300–2300 AU), and $F(r) \propto r^{-1.9}$ between 7 and 20 arcsec (2300–6000 AU).

Most importantly, the large albedo of the dust in the blue shows that this particular dust is smaller than the wavelength with a size $\sim 0.1\mu$m. As mentioned by Kalas & Jewitt, these small grains must be more sensitive to the radiation pressure than to the star gravity and must then be flowing out from the system. Indeed, the central star is a binary system more massive and more luminous than β Pictoris ($2\times5M_\odot$, $2\times830L_\odot$); the ratio of the stellar luminosity to the stellar mass is then 35 times larger for BD+31°643 than for β Pictoris. Particles of size $\sim 0.1\mu$m have a β ratio of radiation force to gravitational force typically 3 to 10 times larger than particles of 1μm size (Burns et al., 1979; Artymowicz 1988). If we simply scale the results of Burns et al. (1979) for the solar system and of Artymowicz (1988) for β Pic to the mass-luminosity ratio of BD+31°643, we find that particles around BD+31°643 have β ratios between 100 and 350.

In fact, the β ratio could even reach ~ 1000 due to the large flux in the UV from a B5V star. With the optical properties given by Draine & Lee (1984) for silicates ("DL silicates") and for graphite, we carried out the β ratio as a function of the size of particles (Fig. 1). We have taken the UV spectrum measured by IUE on two B5V stars used as references (HD 34739 and HD 199081). The radiation pressure coefficient averaged over the stellar spectrum $< Q_{\rm pr} >$ has a major contribution from the flux below 1500Å where the absorption efficiency barely depends on the particle size for particles larger than 0.01μm. Consequently, we find that, in contrast to the solar system case, the β ratio does not reach its maximum at about 0.1μm but around 0.01μm. This shows that particles seen around BD+31°643 must have β ratio larger than $\sim$100 and must be ejected on hyperbolic orbits by radiation pressure.

Gas is also present within the young cluster IC 348 in which BD+31°643 is embedded. Its presence is deduced from spectroscopic observations of absorption lines and from radio maps (Snow et al. 1994). Snow et al. showed that the column density of gas must be $N_{HI} \approx 3 \cdot 10^{21}$ cm^{-2}, which is also consistent with the extinction of the star (E_{B-V}=0.84, $A_V = 2.8$). This allow to obtain observational limits on the gas density in the circumstellar environment. With an observed maximal size of ~ 1 pc for the IC 348 cluster, the gas density has a lower limit $\rho_l \sim 10^3$cm^{-3}. The spectroscopic observations of Snow et al. show that BD+31°643 is inside the cloud. It is also unlikely that the gas density in the star environment is smaller than the mean value in the cluster, because BD+31°643 is at the center of the cluster and coincides with the peak of dust extension and gaseous radio emission map. On the other hand, if the whole column density of the gas was concentrated into the observed disk of size > 2000 AU, we would obtain an upper limit of the gas density $\rho_u \sim 10^5$cm^{-3}.

In short, the observations show that the disk of BD+31°643 has a particular environment with a gaseous medium which density is between 10^3cm^{-3} and 10^5cm^{-3}.

3. Outflow

When a dust particle with $\beta \gg 1$ is produced, it is ejected from the system by radiation pressure. It reaches rapidly a constant asymptotic velocity $v_\infty \sim v_0\sqrt{2\beta - 1}$, where v_0 is the initial velocity of the parent body on its keplerian orbit. Consequently, if some dust is produced close to the star, it is spread in a disk-like structure with a radial density $n \propto r^{-2}$. Nakano (1990) has given the first order relation between the radial distribution of the dust density $n(r)$ and F the apparent surface brightness along the midplane of the disk if seen edge-on from the Earth: $F \propto n(r)r^{-1}$. As a result, the disk produced by outflowing dust has a radial brightness $F \propto r^{-3}$.

But, as already noted in Lecavelier des Etangs et al. (1996a), the gas drag in an edge-on disk decreases the gradient of the observed brightness. The next section is dedicated to the evaluation of the dust distribution taking into account the gas drag.

4. Outflow with gas drag

The motion of one particle driven by the radiation pressure and dragged by the ambient gas is

$$\frac{d\boldsymbol{v}}{dt} = (\beta - 1)\frac{GM}{r^3}\boldsymbol{r} + \boldsymbol{F_{PR}} + \boldsymbol{F_g} \qquad (1)$$

where $\boldsymbol{r}$ and $\boldsymbol{v}$ are the position and the velocity of the particle, M is the mass of the central star, $\boldsymbol{F_{PR}}$ and $\boldsymbol{F_g}$ are the Poynting-Robertson and the gas drags. The Poynting-Robertson effect is negligible compared to the gas drag as soon as the gas density is larger than ~ 1cm^{-3}. The gas drag is given by (Kwok 1975):

$$\boldsymbol{F_g} = -(\sigma/m)m_{\rm H}\mu\rho\sqrt{v_T^2 + (\boldsymbol{v} - \boldsymbol{v_g})^2}(\boldsymbol{v} - \boldsymbol{v_g}) \qquad (2)$$

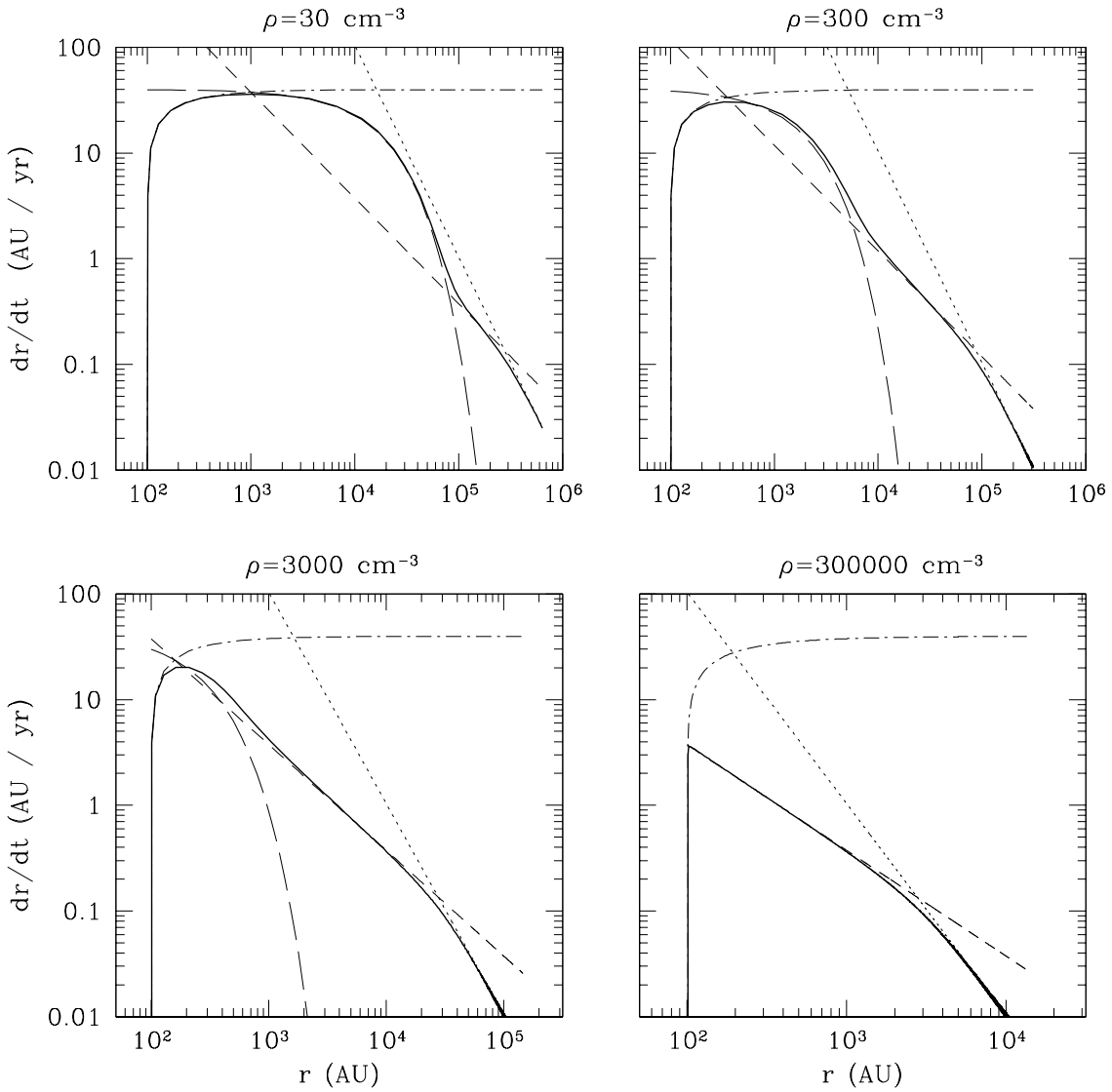

Fig. 2. Plot of the dust radial velocity (dr/dt) as a function of the distance to the star (r) for different gas density (ρ). The dust is supposed to be produced at a distance $r_0 = 100$ AU from the star, the ratio of the radiation force to the gravitational force is $\beta = 200$. The full Eq. 1 has been numerically solved (solid line). The fit to the different phases: acceleration (dot-dashed lines), deceleration (long-dashed line), stationary outflow (short-dashed and dotted lines) are calculated with the approximation given by the equations of Sect. 4.
For $\rho = 30\text{cm}^{-3}$, the particle is accelerated between 100 and 1000 AU; it is then decelerated between 1000 and 10^5 AU and reaches the stationary outflow beyond that point.
For $\rho = 300\text{cm}^{-3}$, the acceleration stops at 300 AU, and the deceleration takes places between 300 and 5000 AU; the stationary outflow starts at $r_2 = 5000$ AU. The distribution changes again at $r_3 = 10^5$ AU when the thermal drag becomes dominant.
For $\rho = 3000\text{cm}^{-3}$, the deceleration phase is very short (between $r_1 = 150$ AU and $r_2 = 400$ AU). The stationary outflow gives a radial velocity $\dot{r} \propto r^{-1}$ (between $r_2 = 400$ AU and $r_3 =$30 000 AU). The velocity regime changes at 30 000 AU beyond which we have $\dot{r} \propto r^{-2}$.
For $\rho = 300\,000\text{cm}^{-3}$, there is no deceleration phase at all. The thermal drag is dominant when $r > r_3 \cong 2800$ AU.

where σ and m are the dust cross section and mass, μ is the mean molecular weight of the gas and $m_{\rm H}$ is the hydrogen mass. v_T is the sound velocity. $\boldsymbol{v_g}$ is the gas velocity and is very small, we have taken $\boldsymbol{v_g} = 0$.

For dust grains, we have $\sigma/m \cong 3/(4s\rho_d)$ where s and ρ_d are the dust size and density. We have shown that $s \propto \beta^{-1}$, where $s\beta \sim 20\mu$m (Sect. 2). Then, with $\rho_d \approx 1$ g cm^{-3}, we obtain $\sigma/m \approx 375\beta$ cm^2 g^{-1}.

From the IRAS 60μm emission we know that the star environment must be at a very low temperature: we can assume $T \sim 30$ K (Snow et la. 1994). Then, as soon as the particle velocity is larger than $v_T = 0.14\sqrt{(T/30\text{K})/\mu}$ AU year^{-1}, the first term under the square root of Eq. 2 is negligible, and assuming $\mu = 1$, we get

$$\boldsymbol{F_g} \approx -375\beta m_{\rm H}\mu\rho|(\boldsymbol{v}-\boldsymbol{v_g})|(\boldsymbol{v}-\boldsymbol{v_g}) \approx -C\beta\rho|\boldsymbol{v}|\boldsymbol{v} \qquad (3)$$

where $C = 9.39 \cdot 10^{-9}\mathrm{cm}^3\mathrm{AU}^{-1}$.

In order to evaluate the radial distribution of dust, we carry out the different phase of the motion by approximate solutions of Eq. 1. We consider only the radial component in the polar coordinates (r, θ) of the vectorial Eq. 1:

$$\frac{d^2r}{dt^2} = r(\frac{d\theta}{dt})^2 + (\beta - 1)\frac{GM}{r^2} - C\beta\rho(\frac{dr}{dt})^2 \quad (4)$$

Since we know that $n(r) \sim \dot{r}^{-1}r^{-2}$, we simply need to determine the radial velocity $\dot{r}$ as a function of the distance to the star, r. Then, the apparent surface brightness along the midplane of the disk, $F \propto n(r)r^{-1}$, can be compared to the observations. If $\beta \gg 1$, the Eq. 4 becomes

$$\frac{d^2r}{dt^2} \approx \beta\frac{GM}{r^2} - C\beta\rho(\frac{dr}{dt})^2 \quad (5)$$

4.1. Acceleration phase

When a particle is produced, its radial distance and velocity are small. Consequently, the last term of Eq. 5 is negligible and we obtain

$$\frac{d^2r}{dt^2} \approx \beta\frac{GM}{r^2}. \quad (6)$$

This gives $\dot{r} = \sqrt{2\beta GM}\sqrt{r_0^{-1} - r^{-1}}$, where r_0 is the initial radial distance at which the dust was produced. This approximation is plotted on Fig. 2 with dot-dashed lines. This is valid for small velocity and small distances, as long as $d^2r/dt^2 > 0$, that is to say for $r < r_1$ where

$$r_1 \equiv \left(r0 + \sqrt{r_0^2 + 2r_0/C\beta\rho}\right)/2. \quad (7)$$

4.2. Deceleration phase

After the particle has gone farther from the star, where the radiation pressure becomes less important, and has gained a large radial velocity, the gas drag becomes dominant and we have

$$\frac{d^2r}{dt^2} \approx -\left(C\beta\rho - \beta\frac{GM}{r^2\dot{r}^2}\right)\left(\frac{dr}{dt}\right)^2 \approx -\alpha\left(\frac{dr}{dt}\right)^2. \quad (8)$$

During this deceleration phase, the first term within parenthesis is largely dominant, and the second term can be considered to be a constant where $r^2\dot{r}^2$ is approximated by its mean value $< r^2\dot{r}^2 >$. Hence, we have $\dot{r} = \dot{r_1}e^{-\alpha(r-r_1)}$.

This approximation is plotted on Fig. 2 with long-dashed lines. This is valid as long as the velocity is large enough for the drag to dominate the radiation pressure. Subsequently, the radial velocity significantly decreases and the drag decreases to the radiation pressure's level. Thus the deceleration takes place when $r_1 < r < r_2$, where r_2 is defined by

$$\dot{r_1}e^{-\alpha(r_2-r_1)} = \sqrt{\frac{GM}{C\rho}}r_2^{-1}. \quad (9)$$

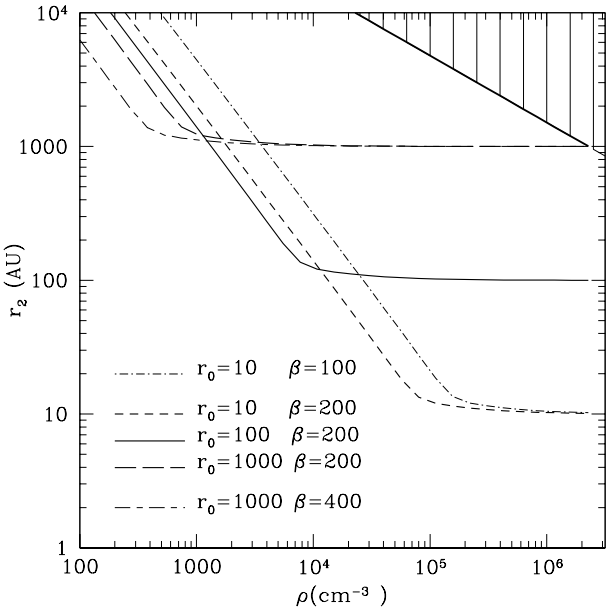

Fig. 3. Plot of the radial distance r_2, as defined in the text. The hashed zone represents the region where $r > r_3$, for a temperature $T = 30$ K. Above the lines representing r_2 and below the hashed zone, we have $\dot{r} \propto r^{-1}$, hence $F(r) \propto r^{-2}$ as observed around BD+31°643 between 2300 and 6000 AU. We see that $r_2 < 2300$ AU gives $\rho \geq 10^3\mathrm{cm}^{-1}$, and $r_3 > 6000$ AU gives $\rho \leq 10^5\mathrm{cm}^{-1}$,

4.3. Stationary outflow

When $r > r_2$, then we simply have $d^2r/dt^2 \sim 0$: this is the stationary outflow where the gas drag exactly compensates the radiation pressure.

From Eq. 5, we get $\dot{r} = \sqrt{\frac{GM}{C\rho}}r^{-1}$. This gives $n(r) \propto r^{-1}$, and $F(r) \propto r^{-2}$, exactly as observed around BD+31°643.

This is represented on Fig. 2 by the short-dashed lines.

When the particle velocity becomes very small, the thermal term is dominant in the gas drag (Eq. 2). This situation occurs when $r > r_3$ where $r_3 \equiv \sqrt{\frac{GM}{C\rho}}v_T^{-1}$. Eq. 5 is then

$$\frac{d^2r}{dt^2} \approx \beta\frac{GM}{r^2} - C'\beta\rho(\frac{dr}{dt}) \quad (10)$$

where $C' = 375m_\mathrm{H}\mu v_T \approx 1.3 \cdot 10^{-9}\sqrt{(T/30\mathrm{K})}\mathrm{cm}^3\mathrm{year}^{-1}$. During this phase, we still have $d^2r/dt^2 \sim 0$, which gives $\dot{r} = \frac{GM}{C'\rho}r^{-2}$, and $F(r) \propto r^{-1}$. This approximation is plotted on Fig. 2 with dotted lines.

5. Application

5.1. The radial velocity versus gas density

We applied the previous calculations and approximations to the case where a grain is produced at a distance $r_0 = 100$ AU from the star and with $\beta = 200$. We have plotted the dust radial velocity (dr/dt) as a function of the distance to the star (r) for different gas density (ρ) (Fig. 2). The full Eq. 1 has been

numerically solved, and the result is given by the solid line in Fig. 2.

The fit to the different phases: acceleration (dot-dashed lines), deceleration (long-dashed line), stationary outflow (short-dashed and dotted lines) are calculated with the approximation given by the equations of Sect. 4. The superposition of the exact solution of Eq. 1 and the different fits validates these approximations and the corresponding domain of application given in the previous section. This also validates the different positions where the changes of regime occur (r_1, r_2, r_3).

For $\rho = 30\text{cm}^{-3}$, we see that the particle is accelerated between 100 and 1000 AU; it is then decelerated between 1000 and 10^5 AU and reaches the stationary outflow beyond that point.

For $\rho = 300\text{cm}^{-3}$, the acceleration stops at 300 AU, and the deceleration takes places between 300 and 5000 AU; the stationary outflow starts at $r_2 = 5000$ AU. The distribution changes again at $r_3 = 10^5$ AU when the thermal drag becomes dominant. This gas density is too low to explain the observed distribution of dust around BD+31°643.

For $\rho = 3000\text{cm}^{-3}$, the deceleration phase is very short (between $r_1 = 150$ AU and $r_2 = 400$ AU). The stationary outflow between 400 AU and (r_3 =)30 000 AU gives a radial velocity $\dot{r} \propto r^{-1}$. Then the disk surface brightness distribution is $F(r) \propto r^{-2}$, exactly as observed around BD+31°643. The distribution changes at 30 000 AU beyond which we have $\dot{r} \propto r^{-2}$, and consequently $F(r) \propto r^{-1}$.

For $\rho = 300\,000\text{cm}^{-3}$, there is no deceleration phase at all. The thermal drag is dominant when $r > r_3 \cong 2800$ AU. This gas density is too large to explain the observed distribution of dust around BD+31°643.

5.2. The BD+31°643 disk

In the BD+31°643 candidate disk, the distribution observed between 2300 and 6000 AU can be explained if the outflow is stationary between r_2 and r_3 as described in Sect. 4.3. This happens only if $r_2 < 2300$ AU and $r_3 > 6000$ AU. In Fig. 3 we have plotted these distances for different ratio β and initial distance r_0. We can see that these conditions are satisfied if we have $10^3\text{cm}^{-1} \leq \rho \leq 10^5\text{cm}^{-1}$.

Incidentally, another solution could be found if the dust is in the stationary outflow in the thermal drag regime ($r > r_3$) and with a radially decreasing gas density $\rho \propto r^{-1}$. In that case, we have $\dot{r} \propto r^{-2}/\rho \propto r^{-1}$, and again $F \propto r^{-2}$. But this would imply that the gas density should be larger than 10^6 cm^{-3} which is incompatible with the observed gaseous column density.

6. Numerical results

For a mixture of particle size (and β), a radial distribution of the sources and the exact treatment of the equation of motion (Eq. 1), numerical simulations are required. We built a code to solve this equation and to calculate the distribution of the dust particles in the steady state of the equilibrium between the continuous replenishment by a distribution of parent bodies and the ejection by the radiation pressure.

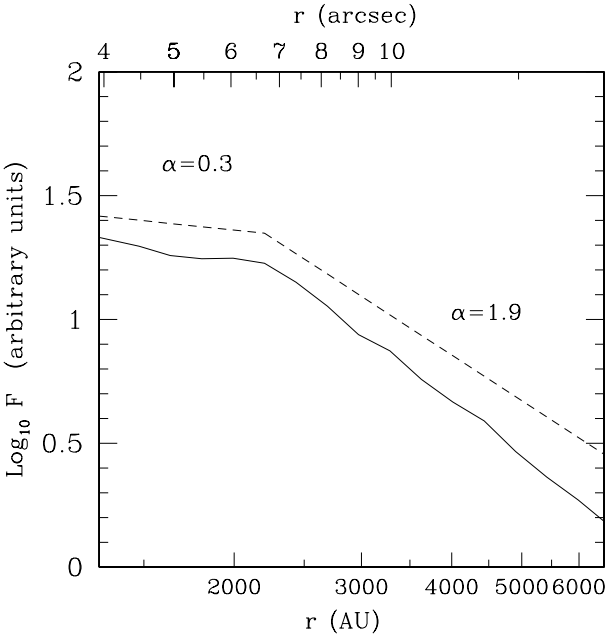

Fig. 4. Brightness distribution of a dust disk seen edge-on and produced by parent bodies on circular orbits between 2000 and 2300 AU. The gas drag is taken into account with $\rho = 10^4\text{cm}^{-3}$. The particles have a β ratio of the gravitational forces to radiation forces between 10 and 1000. This distribution is very close to the surface brightness distribution observed around BD+31°643 by Kalas & Jewitt (1997) (dashed line, slightly arbitrarily shifted to be better compared.)

A wide range of parameters for the dust size distribution, the gaseous density and velocity ($\boldsymbol{v_g}$), and the initial parent bodies positions have been used. The simulations show that dust produced within 2300 AU is able to explain the surface brightness of the disk, provided that the gas density around the star is $\rho \sim 10^4$ cm^{-3}. An example of such a simulation is given in Fig. 4, with a size distribution corresponding to $\beta \in [10, 1000]$. Any size distribution gives the same results, if particles with $\beta \lesssim 10$ are in negligible quantity.

All these parameters are very consistent with the observations of the large albedo of grains in the blue and the estimated density of gas at the center of the cluster IC 348 (Sect. 2). The only parameter newly constrained by these simulations is the position of the parent bodies, which must be located between 2000 and 2300 AU from the star to explain the observed decrease of slope within 2300 AU. It must be mentioned here that BD+31°643 is 200 times brighter than β Pictoris, so that the distance of evaporation of CO (150 AU around β Pictoris) corresponds to about 2100 AU around BD+31°643. But this change of slope can also be linked to the limited resolution of the observations and needs confirmation.

It must also be noted that the velocity of the star relative to the ambient gas ($\boldsymbol{v_*}$) could modify the appearance of the disk. However, as can be inferred from the Fig. 2, simulations show that asymmetries would be visible only for dis-

tances $r \gtrsim 10\,000\ (v_*/1\mathrm{km\,s^{-1}})^{-1}$AU. The observations are thus consistent with the present modeling if $v_* \lesssim 2\mathrm{km\,s^{-1}}$. Considering that the star is at the center of the cluster and that only the transverse motion would give noticeable asymmetries, this last condition is certainly not unlikely.

Finally, the gas drag is the dominant phenomenon which allows to explain the dust radial distribution, but this also rules out the possibility to better constrain the dust origin.

7. Discussion

The dynamics of particles in the BD+31°643 disk and the observed distribution of dust can be explained by the simple model of dust outflow presented here.

Unfortunately, the issue of the origin of the very small particle size remains unexplained. It is not clear why we see so much small particles around BD+31°643, whereas the dust around other main sequence stars with known infrared excess is usually much larger (e.g., Habing et al. 1996).

Also the process which produces these grains is still not determined. The present model of the BD+31°643 disk does not discriminate between production by collision or by evaporation. However, a change of slope and possible inner hole are observed at a distance of 2000 AU, corresponding to the sublimation distance of CO ($\sim$ 2100 AU). Production of dust by evaporation could start if some bodies were heated by the central star after the dissipation of the dense optically thick disk from which a planetary system formed. Alternatively, parent bodies could evaporate if they were scattered planetesimals on eccentric orbits in a forming Oort-like cloud or in a Kuiper-like outer belt (Scattered Icy Objects? Duncan & Levison 1997).

Finally, the particles around BD+31°643 can have a similar origin and nature as the dust grains around β Pictoris, but both disks present different characteristics. The main differences are related to the large distance ratio compensated in part by the larger luminosity of BD+31°643, and consequently the dynamics of dust here expelled by the strong radiation pressure.

Acknowledgements. We are particularly indebted to an anonymous referee for his very useful comments. We would like to express our gratitude to S. Loiseau for his critical reading of the manuscript. We also warmly thank A. Dutrey for very fruitful discussions.

References

Andersson B.G., Wannier P.G., 1997, ApJ 491, L103
Artymowicz P., 1988, ApJL 335, L79
Artymowicz P., 1995, in *Circumstellar Dust Disks and Planet Formation*, Eds. R. Ferlet & A. Vidal-Madjar , p. 335
Artymowicz P., Burrows C., Paresce F., 1989, ApJ 337, 494
Aumann H.H., Gillett F.C., Beichman C.A., et al., 1984, ApJ 278, L23
Benest D., 1998, A&A 332, 1147
Brunini A., 1997, MNRAS 291, 47
Burns J., Lamy P., Soter S., 1979, Icarus 40, 1
Draine B.T., Lee H.M., 1984, ApJ 285, 89
Duncan M.J., Levison H.F., 1997, Science 276, 1670
Habing H.J., Bouchet P., Dominik C., et al., 1996, A&A 315, 233
Kalas P., Jewitt D., 1995, AJ 110, 794
Kalas P., Jewitt D., 1997, Nature 386, 52
Kwok S., 1975, ApJ 198, 583
Lecavelier des Etangs A., Vidal-Madjar A., Ferlet R., 1996a, A&A 307, 542
Lecavelier des Etangs A., Scholl H., Roques F., Sicardy B., Vidal-Madjar A., 1996b, Icarus 123, 168
Lissauer J.J., 1997, Nature 386, 18
Mouillet D., Larwood J.D., Papaloizou J.C.B., Lagrange A.M., 1997, MNRAS, 292, 896
Nakano T., 1990, ApJL 355, L43
Roques F., Scholl H., Sicardy B., Smith B.A., 1994, Icarus 108, 37
Smith B.A., Terrile R.J., 1984, Sci 226, 1421
Snow T.P., Hanson M.M., Seab G.C., Saken J.M., 1994, ApJ 420, 632